Electronic Supplementary Information (ESI) for

Electrochemical nitrogen reduction to ammonia using mesoporous iron oxide with abundant oxygen vacancies

Toshihiro Takashima,*[ab] Takumi Mochida[a] and Hiroshi Irie [ab]

[a.] *Integrated Graduate School of Medicine, Engineering and Agricultural Sciences, University of Yamanashi, 4-3-11 Takeda, Kofu, Yamanashi 400-8511, Japan*
[b.] *Clean Energy Research Center, University of Yamanashi, 4-3-11 Takeda, Kofu, Yamanashi 400-8511, Japan*

Contents

ESI-1) Schematic illustration of an electrochemical cell used in this study.

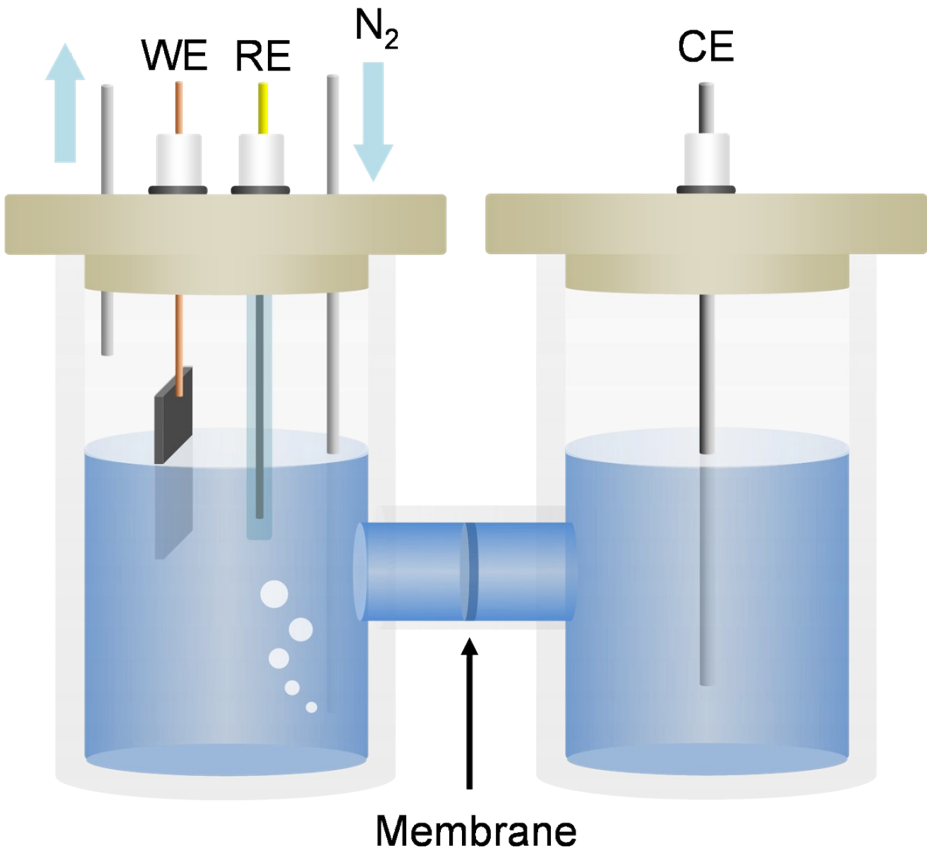

Fig. S1 Schematic illustration of an H-type electrochemical cell used in this study. The electrolyte was continuously purged with N_2 gas throughout the measurements.

ESI-2) Determination of NH_3.

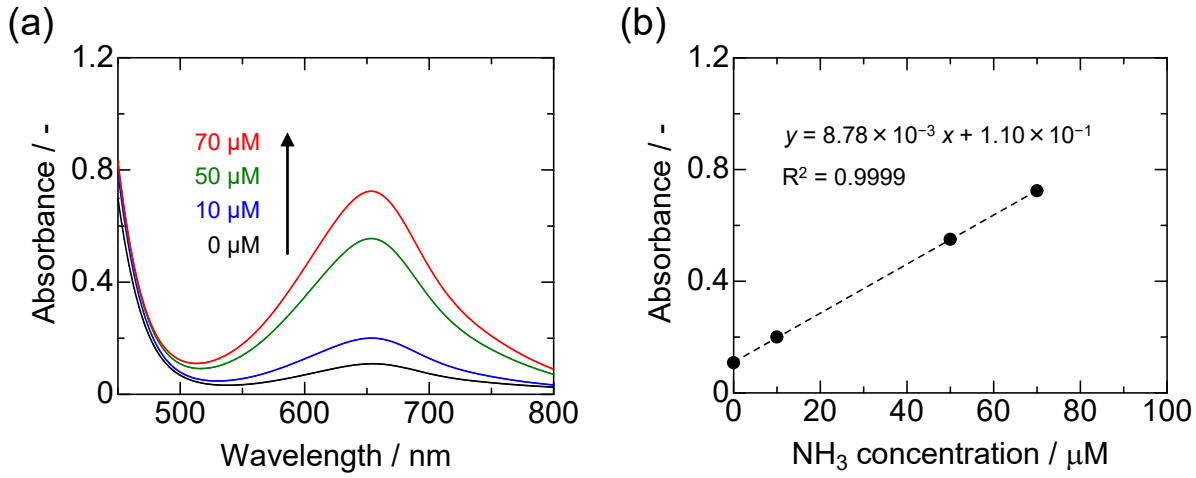

Fig. S2 (a) UV–vis absorption spectra of indophenol assays with NH_4Cl after incubated for 1 h at room temperature. (b) Calibration curve used for calculation of NH_3 concentrations.

ESI-3) Determination of N_2H_4.

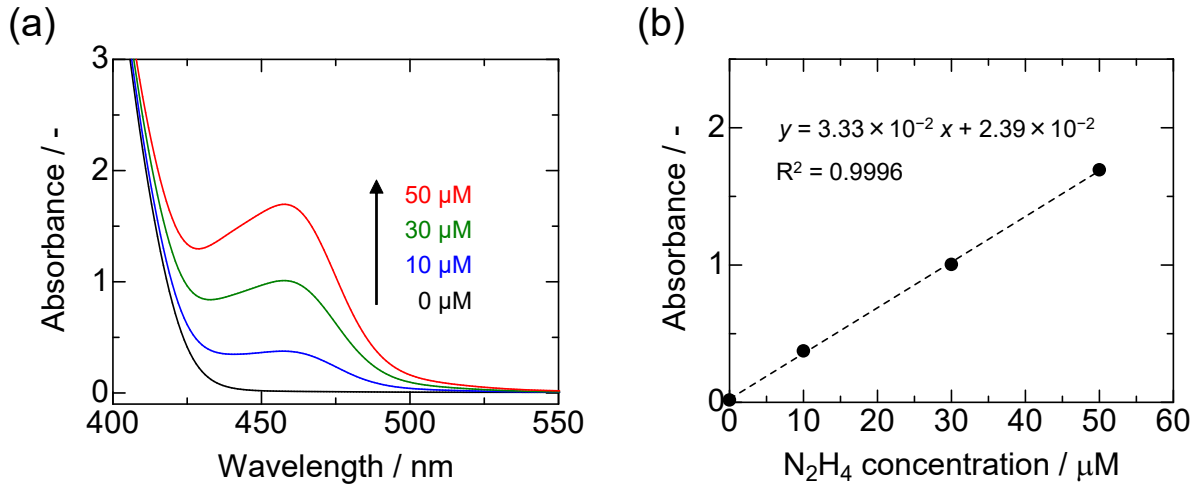

Fig. S3 (a) UV–vis absorption spectra of indophenol assays with N_2H_4 after incubated for 10 min at room temperature. (b) Calibration curve used for calculation of N_2H_4 concentrations.

ESI-4) TEM image of KIT-6 template.

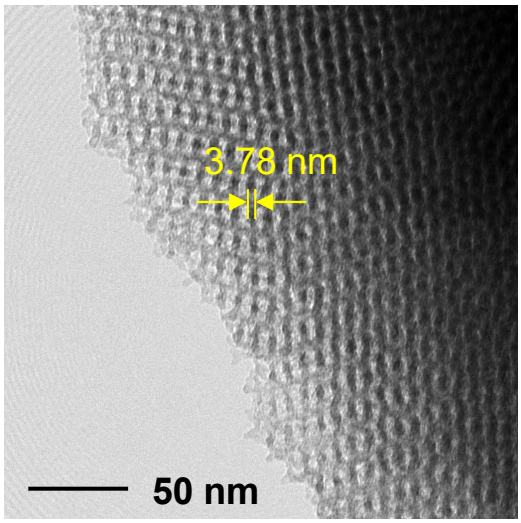

Fig. S4 TEM image of KIT-6 template.

ESI-5) Results of XPS measurements.

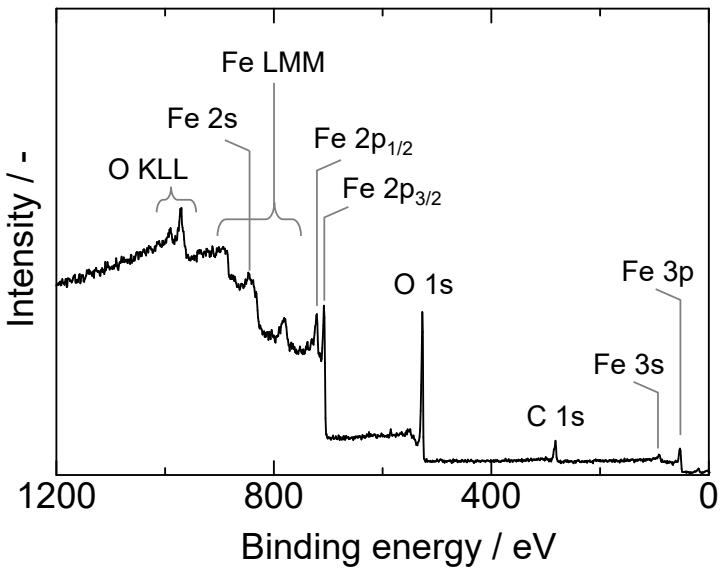

Fig. S5 XPS survey spectrum of meso-α-Fe_2O_3.

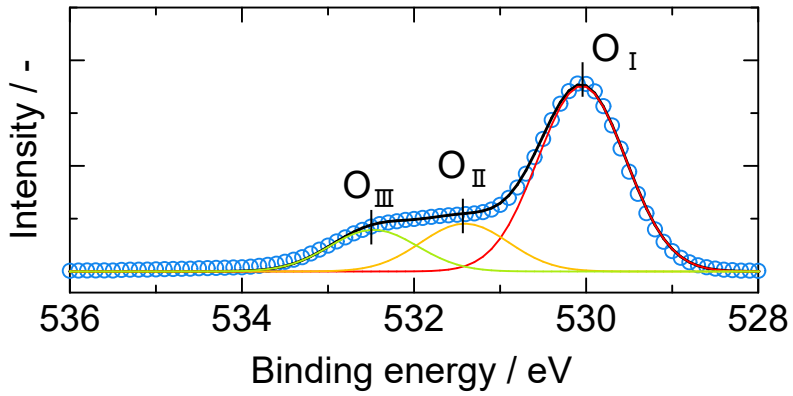

Fig. S6 XPS O 1s spectrum of nano-α-Fe_2O_3 after the KOH treatment.

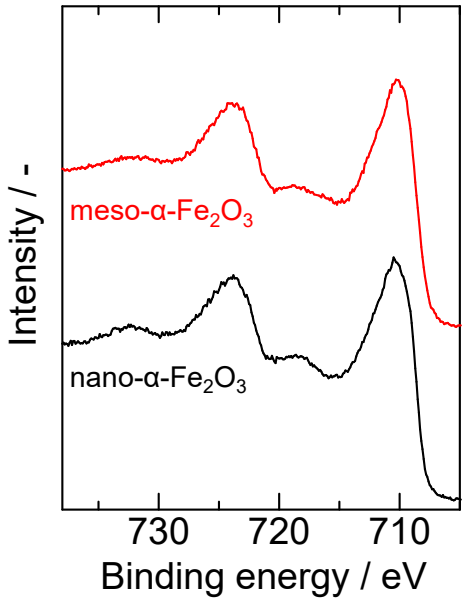

Fig. S7 XPS Fe 2p spectra of meso-α-Fe_2O_3 and nano-α-Fe_2O_3.

ESI-6) H_2 yield and FE of the HER.

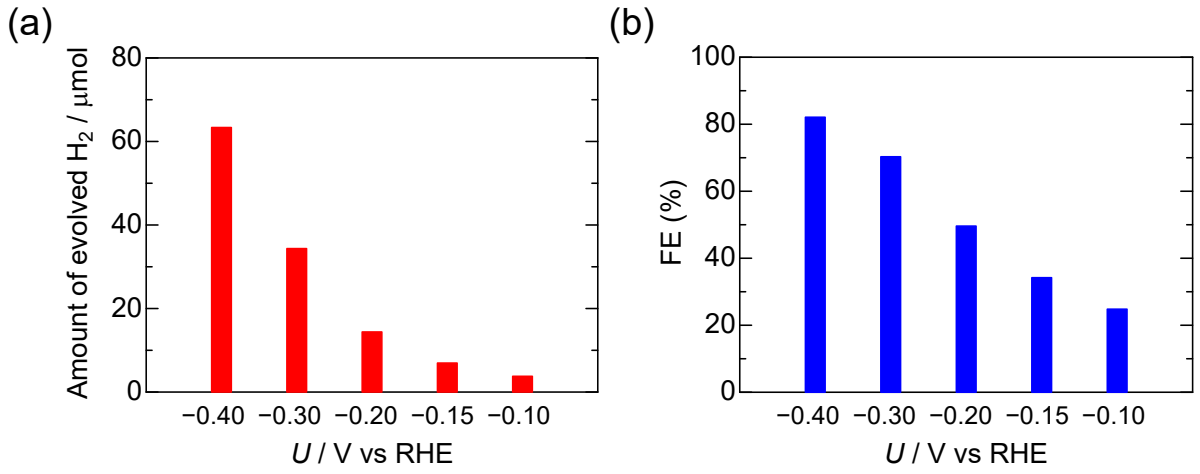

Fig. S8 (a) The amounts of evolved H_2 and (b) the calculated FEs of the H_2 evolution reaction at each given potential.

ESI-7) Characterization of meso-α-Fe_2O_3 after the stability test.

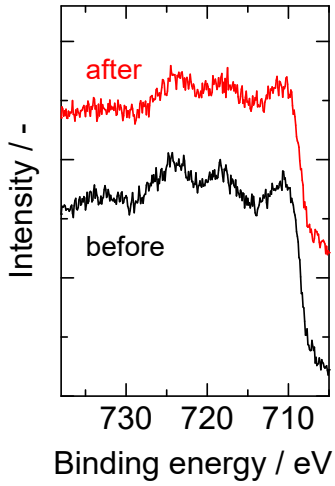

Fig. S9 XPS Fe 2p spectra of meso-α-Fe_2O_3 coated on the electrode before and after the six consecutive cycling tests at −0.15 V.

ESI-8) ECSA determination using electrochemical double-layer capacitance.

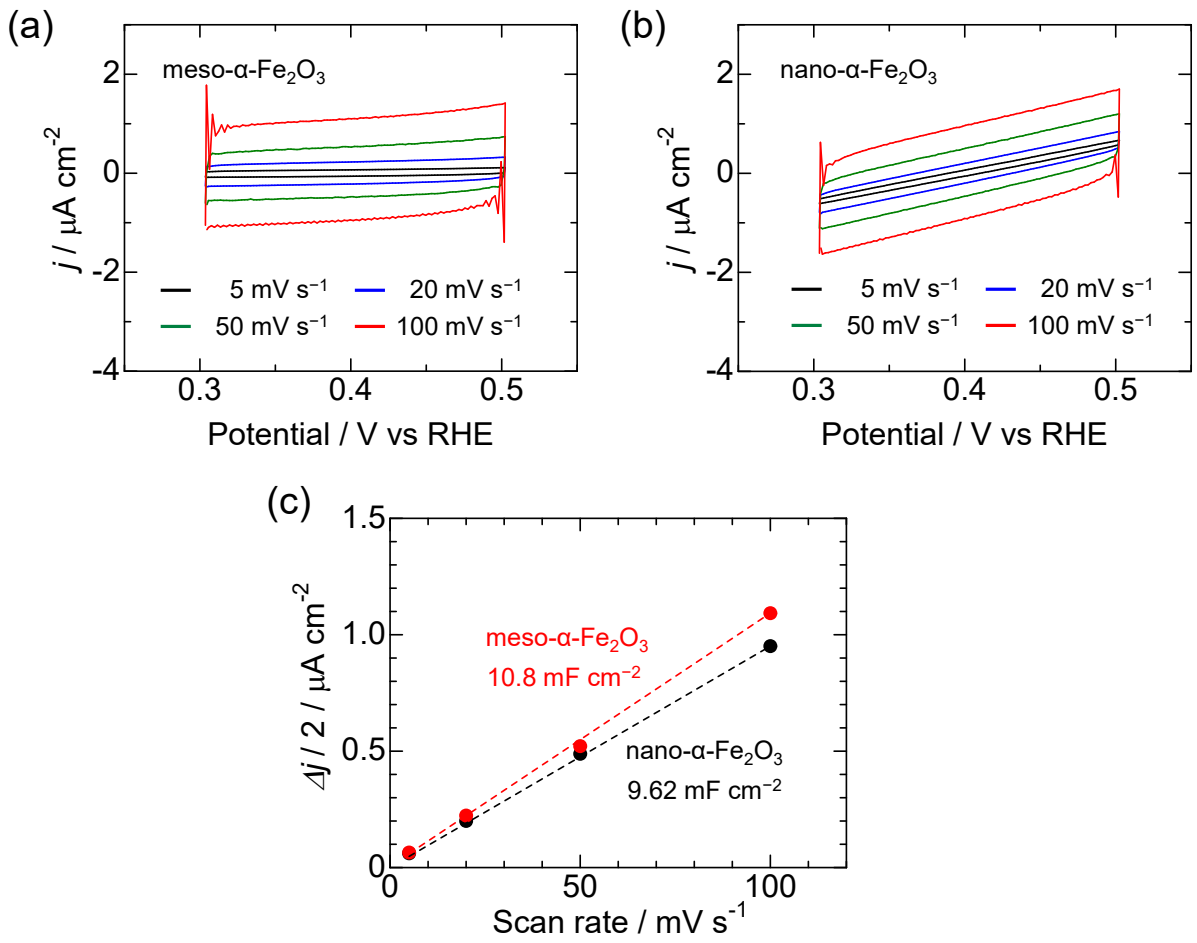

Fig. S10 Cyclic voltamograms of (a) meso-α-Fe_2O_3 and (b) nano-α-Fe_2O_3 at different scan rates, and (c) corresponding plots of current density differences ($\Delta j/2$) at 0.4 V versus scan rate.

ESI-9) N_2-TPD profiles of meso-α-Fe_2O_3 and nano-α-Fe_2O_3.

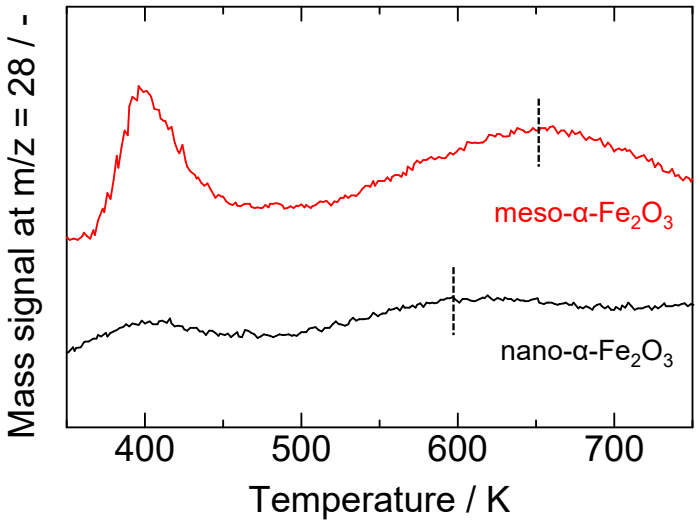

Fig. S11 N_2 temperature-programmed desorption (N_2-TPD) profiles of meso-α-Fe_2O_3 and nano-α-Fe_2O_3. Both samples show two peaks in the range of 350-750 K. The former peak at a lower temperature can be assigned to the desorption of physically adsorbed N_2 and the latter peak at higher temperature can be attributed to the desorption of chemically adsorbed N_2.

ESI-10) Computational calculation details.

Table S1 Calculated zero-point energy (ZPE) and entropy corrections (TS) for all relevant compounds and adsorbed intermediates.

Species	ZPE / eV	TS / eV
N_2(g)	0.27	0.41
H_2(g)	0.15	0.60
NH_3(g)	0.89	0.60
*NN	0.22	0.21
*NNH	0.52	0.14
*NNHH	0.80	0.13
*N	0.09	0.06
*NH	0.45	0.06
*NH_2	0.70	0.08
*NH_3	1.00	0.07

ESI-11) Comparison of NRR performances of Fe-oxide electrocatalysts.

Table S2 Comparison of NRR performances of Fe-oxide electrocatalysts in the literature.

Catalyst	Electrolyte	Potential	NH_3 yield	FE (%)	Ref.
Fe_2O_3/CNT	0.5 M KOH	−2.0 V (vs Ag/AgCl)	0.534 μg h^{-1} cm^{-2}	0.164	[1]
γ-Fe_2O_3	0.1 M KOH	0.0 V (vs RHE)	12.5 nmol h^{-1} mg_{cat}^{-1}	1.9	[2]
o-Fe_2O_3-Ar	0.1 M KOH	−0.9 V (vs Ag/AgCl)	0.46 μg h^{-1} cm^{-2}	6.04	[3]
Fe/Fe_3O_4	0.1 M PBS	−0.3 V (vs RHE)	0.19 μg h^{-1} cm^{-2}	8.29	[4]
Fe_2O_3 nanorod	0.1 M Na_2SO_4	−0.8 V (vs RHE)	15.9 μg h^{-1} mg_{cat}^{-1}	0.94	[5]
rGO/Fe@Fe_3O_4/CP	0.2 M $NaHCO_3$	−0.3 V (vs RHE)	1.3×10^{-10} mol s^{-1} cm^{-2}	6.25	[6]
γ-Fe_2O_3-NC/CF	0.1 M HCl	−0.1 V (vs RHE)	11.7×10^{-10} mol s^{-1} mg_{cat}^{-1}	12.3	[7]
Fe_2O_3/TiO_2/C	1.0 M KOH	−0.577 V (vs RHE)	2.7×10^{-10} mol s^{-1} mg_{cat}^{-1}	0.31	[8]
Fe_2O_3 nanorod/CC	0.1 M Na_2SO_4	−0.4 V (vs RHE)	13.6 μg h^{-1} mg_{cat}^{-1}	7.69	[9]
Fe_2O_3-IL	0.1 M KOH	−0.3 V (vs RHE)	32.1 μg h^{-1} mg_{cat}^{-1}	6.63	[10]
Au/Fe_3O_4	0.1 M KOH	−0.2 V (vs RHE)	21.4 μg h^{-1} mg_{cat}^{-1}	10.5	[11]
Fe_2O_3 NP	0.1 M Na_2SO_4	−0.5 V (vs RHE)	22 μg h^{-1} mg_{cat}^{-1}	3.5	[12]
Fe_3C/Fe_2O_3/Fe/C	6M KOH	0.1 V (vs RHE)	0.3 μg h^{-1} mg_{cat}^{-1}	0.38	[13]
Zn-doped Fe_2O_3	0.1 M Na_2SO_4	−0.5 V (vs RHE)	15.1 μg h^{-1} mg_{cat}^{-1}	10.4	[14]
meso-α-Fe_2O_3	0.1 M Li_2SO_4	−0.15 V (vs RHE)	15.3 μg h^{-1} mg_{cat}^{-1}	13.2	This study

ESI-12) Simulation of proton adsorption.

Table S3 Calculated Gibbs free energy changes (*ΔG*) upon proton adsorption on meso-α-Fe_2O_3 and nano-α-Fe_2O_3.

Catalysts	*ΔG* / eV
meso-α-Fe_2O_3	−0.328
nano-α-Fe_2O_3	−0.329

References

[1] S. Chen, S. Perathoner, C. Ampelli, C. Mebrahtu, D. Su and G. Centi, *ACS Sustain. Chem. Eng.*, 2017, **5**, 7393.

[2] J. Kong, A. Lim, C. Yoon, J. H. Jang, H. C. Ham, J. Han, S. Nam, D. Kim, Y.-E. Sung, J. Choi and H. S. Park, *ACS Sustain. Chem. Eng.*, 2017, **5**, 10986.

[3] X. Cui, C. Tang, X. M. Liu, C. Wang, W. Ma and Q. Zhang, *Chem. Eur. J.*, 2018, **24**, 18494.

[4] L. Hu, A. Khaniya, J. Wang, G. Chen, W. E. Kaden and X. Feng, *ACS Catal.*, 2018, **8**, 9312.

[5] X. Xiang, Z. Wang, X. Shi, M. Fan and X. Sun, *ChemCatChem*, 2018, **10**, 4530.

[6] C. Li, Y. Fu, Z. Wu, J. Xia and X. Wang, *Nanoscale*, 2019, **11**, 12997.

[7] Y. Li, Y. Kong, Y. Hou, B. Yang, Z. Li, L. Lei and Z. Wen, *ACS Sustain. Chem. Eng.*, 2019, **7**, 8853.

[8] R. Manjunatha, A. Karajic, V. Goldstein and A. Schechter, *ACS Appl. Mater. Interfaces*, 2019, **11**, 7981.

[9] Z. Wang, K. Zheng, S. Liu, Z. Dai, Y. Xu, X. Li, H. Wang and L. Wang, *ACS Sustain. Chem. Eng.*, 2019, **7**, 11754.

[10] C. Zhang, S. Liu, T. Chen, Z. Li and J. Hao, *Chem. Commun.*, 2019, **55**, 7370.

[11] J. Zhang, Y. Ji, P. Wang, Q. Shao, Y. Li and X. Huang, *Adv. Funct. Mater.*, 2019, **30**, 1906579.

[12] M. Wang, F. Li and J. Liu, *RSC Adv.*, 2020, **10**, 29575.

[13] J. H. Kim, H. Ju, B. S. An, Y. An, K. Cho, S. H. Kim, Y. S. Bae and H. C. Yoon, *ACS Appl. Mater. Interfaces*, 2021, **13**, 61316.

[14] S. Yu, Q. Wang, J. Wang, Y. Xiang, X. Niu and T. Li, *Int. J. Hydrogen Energy*, 2021, **46**, 14331.